THE JOURNAL OF PHYSICAL CHEMISTRY B
A JOURNAL OF THE AMERICAN CHEMICAL SOCIETY

pubs.acs.org/JPCB

Article

Antiparallel G-Quadruplex Formation Hinders Conversion to a Parallel Topology

Jianjun Xia,[‖] Jielin Chen,[‖] Jiahang Zhou, Mingpan Cheng, Xinzhe Zhuang, Chengfeng Cai, Huangxian Ju, Jean-Louis Mergny, and Jun Zhou*

Cite This: *J. Phys. Chem. B* 2024, 128, 11077−11087

Read Online

ACCESS | Metrics & More | Article Recommendations | Supporting Information

ABSTRACT: G-quadruplexes (G4s) are four-stranded structures formed by guanine-rich sequences. While their structures, properties, and applications have been extensively studied, an understanding of their folding processes remains limited. In this study, we investigated the folding of the sequence $d[(G_3T_2)_3G_3]$ in potassium solutions, focusing on the impact of a folding intermediate on the overall folding process. Our results indicate that this sequence eventually folds into a parallel G4 structure, either directly or through an antiparallel conformation intermediate, suggesting the existence of a specific competitive folding process. Detailed kinetic analysis using stopped-flow techniques reveals that the antiparallel conformation forms much faster than the parallel one. This antiparallel G4 slowly converts to the thermodynamically favored parallel topology, thus slowing the overall folding rate. As a result, the formation of the parallel quadruplex via an antiparallel G4 intermediate is slower than the direct process, indicating that this antiparallel conformation negatively impacts the overall folding process in a temperature-dependent manner. Interestingly, sodium was shown to facilitate the conversion from antiparallel to parallel. These analyses highlight the complexity of the G4 folding process, which is crucial for most biological applications.

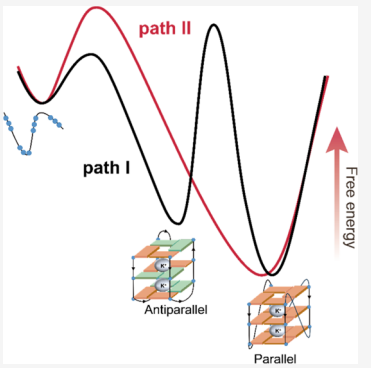

INTRODUCTION

Unlike the base pairs held together by Watson−Crick hydrogen bonds in double-stranded DNA, four guanines can be linked through Hoogsteen hydrogen bonds to form the so-called G-quartet. Stacking of two or more G-quartets via $\pi-\pi$ interactions allows the formation of a G-quadruplex (G4) structure. G4s play critical physiological roles in vivo[1−5] and can be formed by DNA or RNA guanines rich sequences, which display high structural polymorphism. Furthermore, G4-based aptamers have therapeutic potential as drugs for anticancer, antiviral, and anticoagulant agents.[6] However, these G4 aptamers must adopt the correct conformation to function effectively.[7] While the structures and properties of G4s have been extensively studied, including their interactions with ligands, which can stabilize, accelerate folding, or even induce conformational changes,[8,9] much less is known about their folding mechanisms. A number of factors, including temperature, metal ion concentration, ionic strength, and sequence of the loops, influence G4 folding.[10−12] This complexity often complicates direct comparisons across independent studies.

A variety of theoretical and experimental approaches allow studying G4 folding, such as molecular dynamics simulations,[13] ultraviolet−visible absorbance,[14] circular dichroism,[15] nuclear magnetic resonance spectroscopy,[16] fluorescence spectroscopy,[17] infrared spectroscopy,[18] and single-molecule technologies (atomic force microscopy, optical tweezers, magnetic tweezers, and smFRET),[10,14,19] together with stopped-flow[20] and temperature jump techniques.[21] These approaches can be categorized as static or dynamic methods: the former being suitable for describing a stationary (stable) state of G4, while the latter is suitable to investigate transient and continuous processes. Both approaches are commonly combined for the actual characterization of G4 folding.

Existing studies on G4 folding either focus on processes observed in the microsecond (μs) time scale,[22−24] which is appropriate to describe transient processes, or on much longer time scales, in the second (s), minute, or hour range,[11,25,26] to investigate the general folding process. However, less attention has been paid to the millisecond (ms) scale, in between the two time scales discussed above, in which intermediate states may affect G4 folding. Theoretical calculations and experimental data reveal that G4 can experience G-hairpin and G-triplex configurations,[24] and these unstable intermediates form very fast during G4 folding.[22−24] For instance, Chaires and his collaborators demonstrated that human telomeric sequence $A(G_3T_2A)_3G_3$ initially forms a hairpin structure and then

Received: July 8, 2024
Revised: October 23, 2024
Accepted: October 24, 2024
Published: November 5, 2024

https://doi.org/10.1021/acs.jpcb.4c04570
J. Phys. Chem. B 2024, 128, 11077−11087

collapses into an antiparallel G4 structure.[22] Wu et al. used microscale electrophoresis (MST) to investigate the folding process of sequence $T[G_3T_2A]_2T_6G_3$, and the results suggest that G-hairpin and G-triplex intermediates are formed sequentially during the folding process, to finally reach the most stable antiparallel structure.[23] Šponer and colleagues confirmed the existence of parallel G-hairpin and G-triplex species; both are dispensable intermediates that nevertheless play a role in the folding process.[24] In addition, Phan et al. revealed that various factors, including cation, temperature or molecular crowding, etc., can affect G4 folding rate.[11] Chaires and colleagues investigated the effect of metal ions on the G4 folding rate in depth and found that some relatively stable intermediates may have a longer lifetime than the excited state.[27] However, compared with the thermodynamically stable final structure, these intermediate states were stable enough to be significantly populated but still relatively unstable.[27] In fact, the understanding of these unstable structures is often only provided by calculations,[22,28] and more experiments are needed to investigate their contributions to the folding process.

Transient antiparallel G4 structures have been reported in the folding process of several sequences,[22,23,29] and no consensus on their role has been reached until now: are they "dead ends" or real intermediates? Herein, we investigated the contribution of antiparallel G4 structures during the folding process using a stopped-flow technique, based on our previous findings that G4 structure formation by sequences $(G_3T_2)_3G_3$ (shortened as 222 because of its three 2-nucleotide loops) and $T(G_3T_2)_3G_3T$ (shortened as 222T) in K^+ and Sr^{2+} solutions involve two well-defined folded forms.[30] Our results demonstrate that the antiparallel fold acts as a competitor during the folding process rather than as a necessary intermediate. We reveal that 222 and 222T may form parallel structures through two competing pathways: (i) direct folding from a single strand into a parallel structure and (ii) fast antiparallel structure formation, followed by slow interconversion into a parallel structure. This model was supported by (i) the analysis of the control DNA-RNA chimeric sequence GgGTTgGgTTGgGTTgGg (shortened as d222r, ribonucleosides and deoxyribonucleosides indicated by lower- and uppercase letters, respectively), which cannot adopt an antiparallel structure and (ii) our observations of 222 folding in K^+ at higher temperature (60 °C) for which no antiparallel structure is observed. We analyzed the properties of this antiparallel G4 structure and found that its competition efficiency depended on temperature and the nature of metal ions. These analyses reveal the role of the antiparallel G4 topology in DNA G4 folding.

MATERIALS AND METHODS

DNA Oligonucleotides. HPLC-purified DNA oligonucleotides were purchased from Sangon Biotech (Shanghai, China). To ensure the sequences remain single-stranded before the experiments, the sequences were dissolved in 10 mM Tris-HCl buffer (pH 7), 5 mM LiOH was added, and the mixture was heated at 95 °C for 30 min next; then, the pH was adjusted to neutrality by HCl. Finally, the samples were stored at 4 °C for future experiments. The concentrations of oligonucleotides were estimated using the UV absorbance at 260 nm and the extinction coefficients provided by the manufacturer.

Circular Dichroism (CD). The steady-state CD experiments were performed on a JASCO J-1500 spectropolarimeter with a Peltier accessory to control the temperature. The samples were prepared at 10 μM strand concentration with or without 100 mM cations, heated at 95 °C for 5 min, and then slowly annealed to room temperature and incubated overnight at 4 °C before measurements. For the CD spectra, a cuvette with a 2 mm path length was used, and every sample was tested thrice from 220 to 320 nm. The obtained spectrum was averaged after the subtraction of the corresponding buffer.

The dynamic experiments were conducted on the same CD spectropolarimeter with the SFS-562T module, which can perform dynamic measurements between 5 and 80 °C. The dead time of the sample injection device is 100 ms, and the measurement time, time interval, and DIT are determined automatically by the actual measurement situation. The DNA and cation concentrations used for stopped-flow measurement were 10 μM and 100 mM, respectively. For subsequent high-quality singular value decomposition (SVD) analysis, multiple measurements were performed to reduce the error. Specifically, the number of detection groups was inversely correlated with the measurement time in order to mitigate excessive errors resulting from the limited duration of the measurements.

Singular Value Decomposition (SVD) Analysis. To calculate the number of reaction stages of G4 formation, multiple sets of kinetic curves collected through residence were formed into a large matrix $D_{i,j}$ (each column represents the CD intensity of different groups of measurement wavelengths at the same time, and each row represents the CD intensity of the same group over time). Singular value decomposition on $D_{i,j}$ was run using Wolfram Mathematica 13.2, and three matrices were obtained: U (basis spectra), S (singular values), and V (the amplitude vector of the time function).

$$D = S \times U \times V \tag{1}$$

Each singular value was sorted based on the magnitude of the variance value. For those components, a variance value of ≤0.5% was not considered as significant in dynamic measurements. The number of reaction stages was determined based on the obtained singular and variance values.

The screen plot, a chart that associates each component with its singular value, was mapped by using all generated singular values. The total relative variance (RV) was obtained by the variance S_i corresponding to each singular value. The principal components were identified as those with a cumulative variance sum ($\sum_i Si$) of 99% or higher.

$$\mathrm{RV} = \frac{S_i}{\sum_i S_i} \tag{2}$$

Calculation of Dynamic Constants. To analyze dynamic constants, four possible folding scenarios listed below were considered:

$$\text{(I)}\ \mathrm{UF} \rightleftharpoons \mathrm{F_2} \tag{3}$$

$$\text{(II)}\ \mathrm{UF} \rightleftharpoons \mathrm{F_1} \rightleftharpoons \mathrm{F_2} \tag{4}$$

$$\text{(III)}\ \mathrm{F_1} \rightleftharpoons \mathrm{UF} \rightleftharpoons \mathrm{F_2} \tag{5}$$

$$\text{(IV)}\ \mathrm{F_2} \rightleftharpoons \mathrm{UF} \rightleftharpoons \mathrm{F_1} \rightleftharpoons \mathrm{F_2} \tag{6}$$

where UF, F_1, and F_2 refer to unfolded structure, antiparallel, and parallel G4 conformations, respectively. It should be noted that the unfolded state cannot be considered as an independent species in SVD analysis. As the CD signal and the G4 concentration obey approximately a first-order linear

https://doi.org/10.1021/acs.jpcb.4c04570
J. Phys. Chem. B 2024, 128, 11077−11087

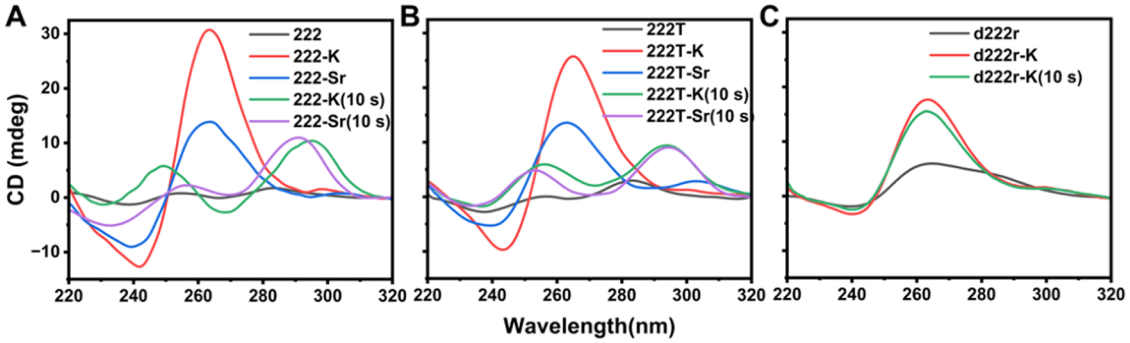

Figure 1. CD spectra of 10 μM (A) 222 and (B) 222T without cations (black), in the presence of 100 mM K^+ (red) or Sr^{2+} (blue) after the addition of cations in 10 s (green and purple, respectively), and the corresponding fully folded structures prepared by typical procedure, that is heated at 95 °C, then incubated at 4 °C overnight; (C) CD spectra of 10 μM d222r for control, and the conditions are same to above except Sr^{2+} was not used here. The color legends in panel (C) are the same as those in panels (A, B). All of the experiments were performed in 10 mM Tris-HCl buffer (pH 7) at 25 °C.

relationship, the folding process can be studied through the changes of the characteristic peaks of CD spectra. The intramolecular G4 folding process is a pseudo-first-order reaction, which can be determined by the below-mentioned first-order reaction kinetics formula:

$$k = -\mathrm{d}c/\mathrm{d}t \tag{7}$$

where k and $\mathrm{d}c/\mathrm{d}t$ refer to the rate constant and the change in concentration of monomer over time, respectively. The rate constants were calculated by the fitting formula 11 described below, which is based on a model by tracking the time dependent CD signal of at least two G4 characteristic peaks.

Calculation of Thermodynamic Constants. The usual methods, like UV thermal melting, are not suitable to calculate the thermodynamic constants of intermediates due to their limited lifespan. To solve this problem, a new thermodynamic constant calculation method based on the CD signal of species at unit concentration was established in this work. In the process of kinetic fitting, we calculated the CD signal of the species at unit concentration. The concentrations of each species were calculated from the fully folded CD spectrum and the CD intensity per unit concentration of different species:

$$[\mathrm{UF}] = [\mathrm{CD}_i]_{\mathrm{UF}} \quad [\mathrm{F}_1] = [\mathrm{CD}_i]_{\mathrm{F}_1}/A_2 \quad [\mathrm{F}_2] = [\mathrm{CD}_i]_{\mathrm{F}_2}/A_3 \quad /A_1 \tag{8}$$

where $[\mathrm{UF}]$, $[\mathrm{F}_1]$, and $[\mathrm{F}_2]$ refer to the concentrations of UF, F_1, and F_2, respectively; $[\mathrm{CD}_i]_{\mathrm{UF}}$, $[\mathrm{CD}_i]_{\mathrm{F}_1}$, and $[\mathrm{CD}_i]_{\mathrm{F}_2}$ represent the CD intensities of UF, F_1, and F_2, respectively; A_1, A_2, and A_3 refer to the CD intensities of 10 μM UF, F_1, and F_2, respectively. According to the equilibrium constant formulas:

$$K^\circ = [\mathrm{F}_1]/([\mathrm{F}_2] \times [\text{metal ion}]) \tag{9}$$

$$K^\circ = k_{\mathrm{on}}/k_{\mathrm{off}} \tag{10}$$

where K° refers to the equilibrium constant of the folding process and [metal ion] represents the concentration of the metal ion. The equilibrium constant can be obtained by forward and inverse reaction rate constants, k_{on} and k_{off}. In addition, the activation energy of forward and reverse reactions can be calculated using the Arrhenius equation:

$$\ln k = -E_a/RT + C \tag{11}$$

where E_a refers to the activation energy of the folding process and T, R, and C refer to temperature, gas constant, and dimensionless constant, respectively. Furthermore, the thermodynamic constants ΔG can be calculated from the standard Gibbs function (12):

$$\Delta G^\circ = -RT \ln K^\circ \tag{12}$$

where ΔG° represents Gibbs free energy.

RESULTS

Folding of 222 and 222T. Previous data showed that 222 and 222T form antiparallel G4 structures in sodium and low concentrations of K^+.[30] In contrast, they adopt parallel structures at high concentrations of K^+.[30] In another work, we also found that 222 and 222T rapidly form antiparallel G4 structures and then transit into a parallel topology in 100 mM K^+.[31]

CD spectra were collected to identify the structures of 222 and 222T under different experimental conditions. As displayed in Figure 1A,B, 222 and 222T exhibit a very similar behavior. For instance, both remain single-stranded in the absence of cations and (within 10 s) form antiparallel G4 structures rapidly after addition of 100 mM K^+ or 100 mM Sr^{2+}, with characteristic positive and negative peaks around 295 and 265 nm, respectively. In contrast, when using a typical annealing procedure (heating at 95 °C in the presence of cations, followed by slow cooling to room temperature and storage at 4 °C overnight), both exhibit positive and negative peaks at 264 and 242 nm, respectively, demonstrating the formation of a parallel G4 structure corresponding to the thermodynamically favored species.[30] These CD results imply that the antiparallel G4 structure may constitute an intermediate species in the folding process of parallel G4, which was supported by NMR results that single-stranded DNA was converted into a single G4 structure quickly (Figure S1). To verify our hypothesis, we designed a chimeric DNA-RNA sequence d222r, in which guanines adopt *syn*-glycosidic bonds in the 222 antiparallel conformations that were replaced by RNA bases. d222r can only form a parallel G4 structure as the 2′−OH group in RNA favors the *anti*-conformation of guanine residues.[32] The CD spectra of d222r under the same conditions as those of 222 and 222T are displayed in Figure 1C. No antiparallel structure similar to 222/222T was observed.

https://doi.org/10.1021/acs.jpcb.4c04570
J. Phys. Chem. B 2024, 128, 11077−11087

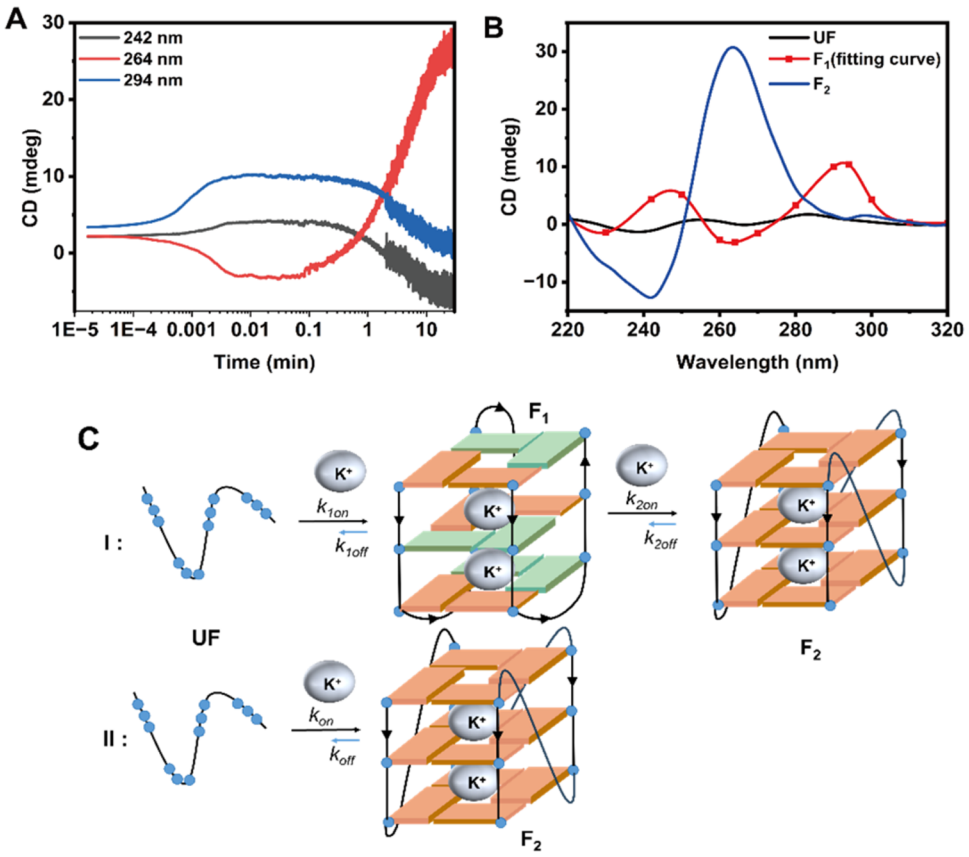

Figure 2. (A) Time-tracking curves of 10 μM 222 in 100 mM K^+ at 242 nm (black), 264 nm (red), and 294 nm (blue), respectively. The experiments were performed in 10 mM Tris-HCl buffer (pH 7) at 25 °C. (B) CD spectra of UF, F_1, and F_2. A single strand of 222, named as UF (black); 222 partly and completely folded into an intermediate and G4 structure in 100 mM K^+, named as F_1 (red) and F_2 (blue), respectively. Note: CD spectrum of F_1 is the fitting curve. (C) Folding model of sequence 222/222T in a K^+ solution. Path (I) corresponds to single-stranded DNA forming an antiparallel G4 structure first, followed by a switch to a parallel conformation; in Path (II), the unfolded structure forms a parallel G4 structure directly. Guanines in *anti* and *syn* conformations are colored orange and green, respectively.

Evidence of Antiparallel Structure and Its Role in the Folding Process. The purpose of this study was to validate the antiparallel structure of the intermediate form and investigate the formation process. To do so, we recorded with a stopped-flow apparatus the time-tracking curves of CD spectra of 222 at 242, 264, and 294 nm in 100 mM K^+ at 25 °C. These three wavelengths correspond to the typical peaks of parallel and antiparallel G4s. The time-tracking curves are summarized in Figure 2A, and the original time-tracking curve data are shown in Figure S2.

To validate the factors that affect the folding process,[20,33] singular value decomposition (SVD) analysis was performed to decompose the time-tracking curves of CD spectra. As displayed in Table 1, three sets of wavelengths (242, 264, and 294 nm), each set with 50 time-tracking curves, were analyzed. The results show that there are two main factors (with eigenvalues of 1031 and 163.7, respectively) affecting the variation of the time-tracking curves. It is worth noting that the single strand has a weaker peak and thus a smaller eigenvalue ($\ll$163.7), but it is still a species in the G4 folding process. Therefore, three main species were considered in the G4 folding process: (i) the unfolded structure UF, (ii) the fully folded parallel G4 structure F_2, and (iii) the antiparallel intermediate structure F_1. Four possible models shown in Table S1 were compared based on the above results. The fitting analysis results revealed that the fourth model, in which the unfolded structure (UF, single strand) forms either directly the parallel G4 structure (F_2) or via an antiparallel intermediate structure (F_1) which then transforms into parallel topology (F_2), is the best one to fit the data. This model reasonably explains the possible folding process of 222 in K^+, while the three others do not. The first model (single strand directly forms a parallel structure) is unable to reflect the effect of the antiparallel intermediate structure on the folding process. The second model (single strand forms the antiparallel intermediate structure and then transforms into parallel topology) could not explain the folding process of 222 at 65 °C (the data shown in subsequent Figure 3A). The third model (single strand forms antiparallel intermediate or parallel simultaneously) cannot explain why the parallel structure is the overwhelmingly predominant topology observed. The fourth model can be simplified into the first one at high temperatures

Table 1. SVD Analysis Results of 222 in K^+

time scale	number	eigenvalue	variance (%)	cumulative variance (%)
2 min	1	1031	85.83	85.83
	2	163.7	13.63	99.46
	3	1.045	0.087	99.54
	4	0.985	0.082	99.63
5 s	1	9901	99.00	99.00
	2	28.09	0.281	99.28
	3	10.42	0.104	99.38

https://doi.org/10.1021/acs.jpcb.4c04570
J. Phys. Chem. B 2024, 128, 11077−11087

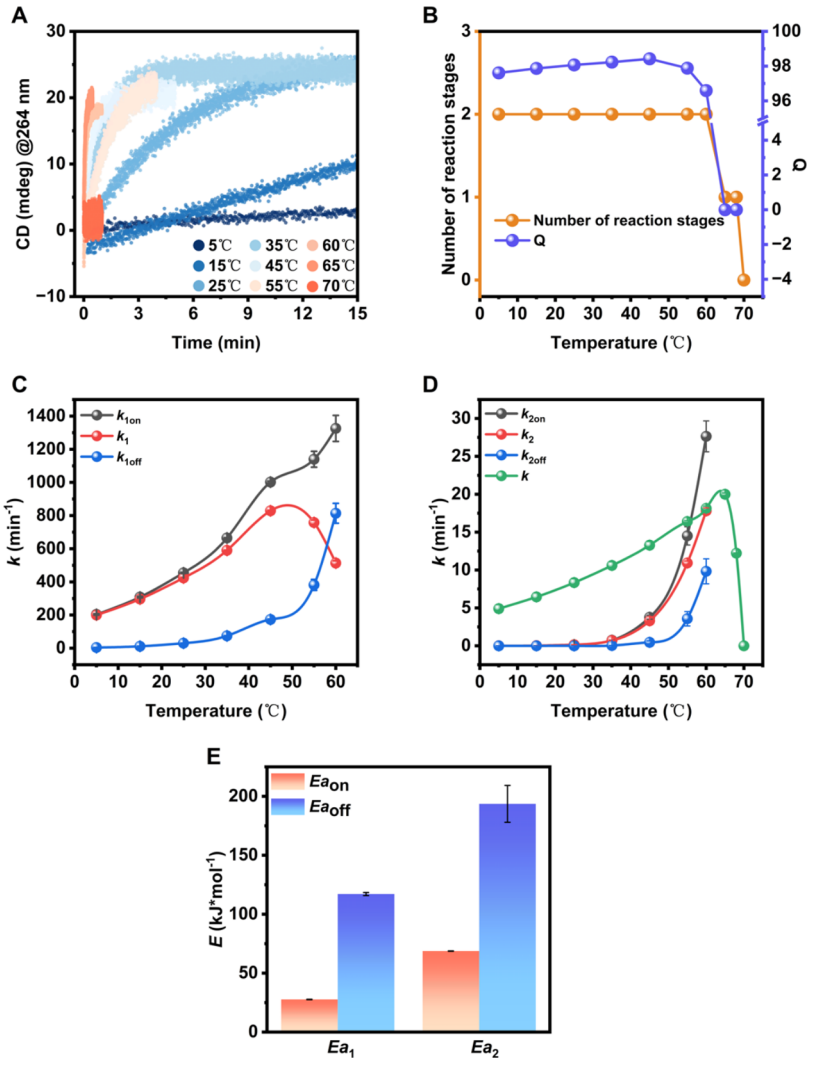

Figure 3. (A) Time-tracking curves of the 10 μM sequence 222 at 264 nm with 100 mM K^+ at different temperatures (5, 15, 25, 35, 45, 55, 60, 65, and 70 °C). The experiments were performed in 10 mM Tris-HCl buffer (pH 7). (B) Number of reaction stages and Q of the 10 μM sequence 222 with 100 mM K^+ at different temperatures. The blue and brown lines represent the competitiveness of the antiparallel structure F_1 and the number of reaction stages of 222 as a function of temperature, respectively. (C) Effect of temperature on the total rate constant k_1 (red) and forward and reverse reaction rate constants k_{1on} (black) and k_{1off} (blue). (D) Variation of total rate constant k_2 (red), k (green), forward and reverse reaction rate constants k_{2on} (black), and k_{2off} (blue) with temperature (for temperatures ≤55 °C, k is calculated by the Arrhenius formula). (E) Forward and reverse activation energies for the two reactions of the folding process I. In folding process I, E_{a_1} is the activation energy of UF → F_1; E_{a_2} is the activation energy of F_1 → F_2. $E_{a_{on}}$ is the activation energy of the forward reaction, and $E_{a_{off}}$ is the activation energy of the reverse reaction.

(see details below). It should be noted that putatively, very early and transient (μs scale) species are not considered in these models, as stopped-flow methods are not resolutive enough to analyze phenomena in this time range.

The fitting results of 222 in K^+ give folding rate constants k_1 and k_2 of 424.2 and 0.1500 min^{-1} (Figure S3), respectively, and k is 8.345 min^{-1}. Furthermore, the CD intensity of F_1 was obtained by fitting the time-tracking curves. For example, F_1 exhibits a CD intensity of 4.4 at 242 nm, −3.1 at 264 nm, and 10.4 at 294 nm. In order to obtain a complete CD spectrum of F_1,[22] the time-tracking curves were measured at 10 nm intervals in the range of 220 to 320 nm. The CD spectra of UF and F_2 and the fitting curve of F_1 are displayed in Figure 2B. The fitted CD spectrum of F_1 agrees with an antiparallel G4 structure. The model of the whole folding process is shown in Figure 2C, and the folding process is divided into two paths: (I) UF → F_1 → F_2, (II) UF → F_2. The unfolded structure can be first folded into an antiparallel G4 structure, which then undergoes a conformational transformation to form a parallel structure. In addition, the unfolded structure can be directly folded into a parallel structure simultaneously. Since $k_1 \gg k$, the antiparallel G4 structure is much faster to form than the parallel structure. In order to better understand this competitive effect, Q was introduced here to evaluate the competitive ability of antiparallel G4 structures, which was calculated as below (formula 13):

$$Q = k_1/(k_1 + k) \tag{13}$$

Q has a physical significance, as it reflects the ratio of antiparallel structures to the total amount of all G4s at transient equilibrium (F_1 without conformational transitions and all of UF undergoes folding). Larger values of Q indicate that the antiparallel structures are more competitive in the folding process. Since $k_1 \gg k_2$, the conformational transition

https://doi.org/10.1021/acs.jpcb.4c04570
J. Phys. Chem. B 2024, 128, 11077−11087

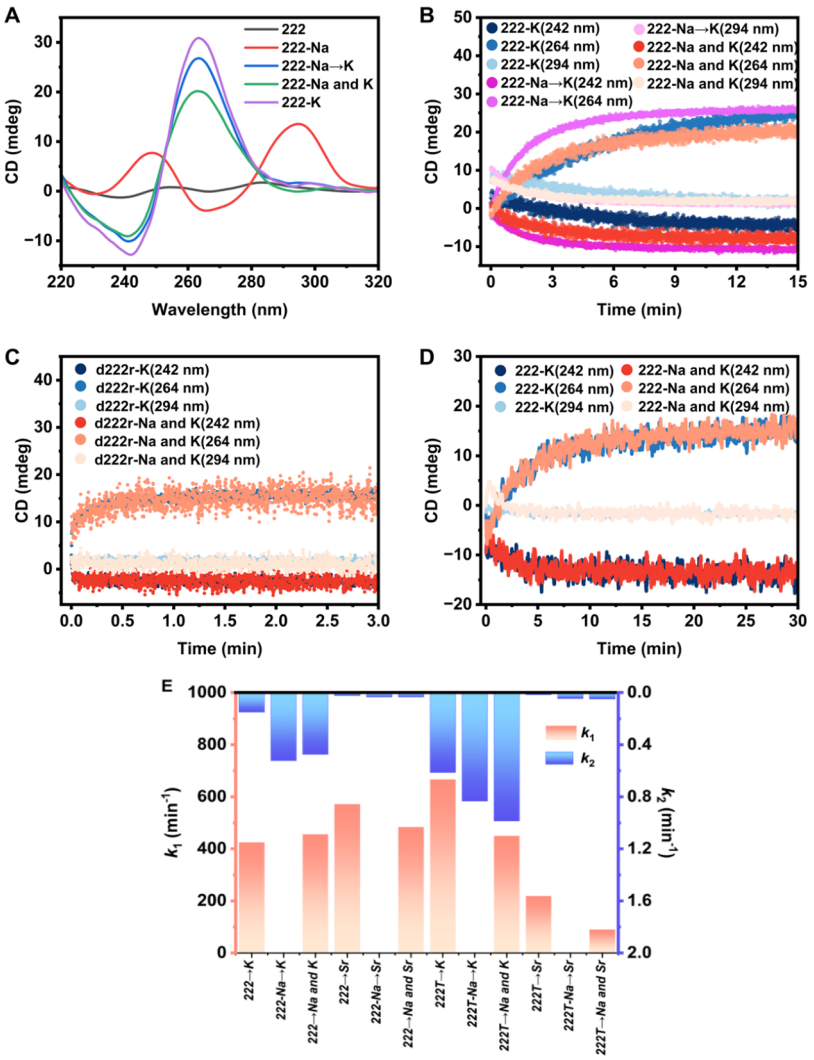

Figure 4. (A) CD spectra of 222 (black), 222 in Na^+ (red), 222 in Na^+ solution first then adding K^+ (blue), 222 in solution with Na^+ and K^+ simultaneously (green), and 222 in K^+ (purple) at 25 °C. (B) Time-tracking curves of 222 in K^+, 222 in Na^+ after addition of K^+, and 222 in Na^+ and K^+ mixed solution at 25 °C. The folding rate of 222 in K^+ can be accelerated by the introduction of Na^+ but independent of the addition order of Na^+. (C) Time-tracking curves at 242, 264, and 294 nm of d222r in K^+ and in Na^+ and K^+ mixed solution at 25 °C. The folding rate of d222r in K^+ cannot be accelerated by the addition of Na^+ because d222r is unable to form an antiparallel structure, and Na^+'s role is to accelerate the antiparallel to parallel conformational transition. (D) Time-tracking curves at 242, 264, and 294 nm of 222 in K^+ and 222 in Na^+ and K^+ mixed solution at 65 °C. The folding rate of 222 in K^+ cannot be accelerated by the introduction of Na^+ at 65 °C. The reason is that 222 folds at 65 °C using path II, which does not involve an antiparallel structure. The sequence concentrations are 10 μM, and the concentrations of K^+ and Na^+ are 100 mM. (E) Rate constants of 222 and 222T in different metal ion environments. Note: the rate constant for 222/222T in 100 mM Na^+ after the addition of 100 mM KCl or $SrCl_2$ is unavailable for k_1 because no antiparallel structure formation occurs. All of the experiments were performed in 10 mM Tris-HCl buffer (pH 7).

($F_1 \rightarrow F_2$) is the rate-limiting step of path I during the folding process. Moreover, the parallel structure folds faster through path II than through path I due to $k \gg k_2$. Interestingly, the folding processes of 222 in Sr^{2+} (Figure S4 and Table S2) and 222T in K^+ (Figure S5 and Table S3) and Sr^{2+} (Figure S6 and Table S4) are similar to the one of 222 in K^+: they all conform to the model shown in Figure 2C, suggesting the generality of the phenomena.

Properties of Antiparallel Intermediate G4 Structures. To demonstrate the role of the antiparallel G4 structure in the folding process, we selected d222r as a control. Two major species, one of which does not contribute to the CD spectrum, were identified by SVD analysis for the d222r folding process (Table S5). The first model in Supporting Table S1 was therefore used to fit the time-tracking curve of d222r, and the calculated rate constant k was 10.44 min^{-1}, which is approximately 70-fold faster than that of its corresponding all-DNA parent sequence, 222 in K^+. This result confirms that the antiparallel G4 structure acts as a competitive species in the folding process. Next, the nature of the antiparallel G4 structure was explored.

Effect of Temperature on Antiparallel Intermediate G4 Structure. F_1 being a very short-lived structure, it is difficult to determine its T_m directly; therefore, we developed a strategy to determine the temperature at which the antiparallel G4 structure disappears by determining the folding process of 222 in different temperature gradients. As displayed in Figures 3A and S7, the time-tracking curves of 222 folding in 100 mM K^+ at 5−70 °C were measured separately (the melting temperature of 222 is 70 °C, as shown in Figure S8).

https://doi.org/10.1021/acs.jpcb.4c04570
J. Phys. Chem. B 2024, 128, 11077−11087

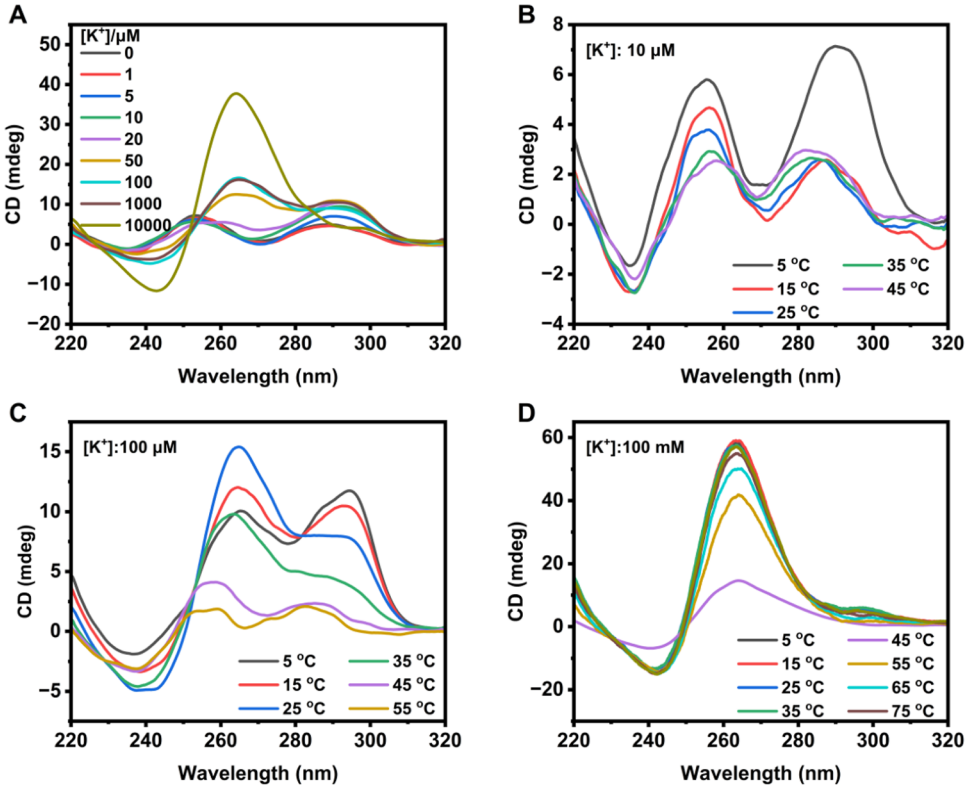

Figure 5. CD spectra of 10 μM 222 (A) at 25 °C with different concentrations of K^+ and at different temperatures with various concentrations of K^+: (B) 10 μM, (C) 100 μM, and (D) 100 mM. The conformation of 222 changes with temperature and the potassium concentration. 222 tends to form antiparallel structures at low concentrations of K^+, and low temperatures are more favorable to the formation of antiparallel structures.

Decomposition of these time-tracking curves on a time scale using SVD yielded the number of reaction stages (i.e., reactant species-1) at different temperatures (Figure 3B). As envisioned earlier, when the temperature is less than or equal to 63 °C, the reaction proceeds in two stages, while the reaction involves only one stage at a temperature higher than 65 °C (but lower than 70 °C). We observed a gradual disappearance of characteristic peaks of antiparallel structure between 63 and 65 °C. Therefore, we hypothesize that the T_m value for the antiparallel G4 structure is in the range of 63 °C−65 °C. The antiparallel structure will disappear when the temperature is higher than its T_m during the folding process. The competitive ability of F_1 enhanced and then decreased with increasing temperature, but always remained high (Figure 3B). When the temperature increased to 65 °C, F_1 lost its competitive ability, and the parallel G4 could only fold through pathway II. Then, at even higher temperatures (exceeding the T_m of parallel G4), folding could not occur as excepted.

Based on the results of the SVD analysis described above, the model was fitted sequentially for 5−60 °C and above 65 °C using models 4 and 1 in Table S1 (k_1 = 0 in model 4), respectively. The temperature dependence curves of the rate constants are shown in Figure 3C,D. The experimental results show that k_1 first increases and then decreases with temperature, but its value is always much higher than that of k_2 and k. The equilibrium constants for the folding process were obtained by measuring the concentration of each species at the reaction end point (Table S6). The equilibrium constant of G4 folding decreases as temperature increases, which is consistent with the expected conclusion that G4 formation is enthalpy-driven and, therefore, more stable at low temperatures.[34]

To measure the unfolding rate constants of F_1 and F_2, an equivalent amount of complementary sequence C222 (5′-CCCAACCCAACCCAACCC-3′) was added to sample 222 at different times, either 1 min after K^+ addition (conditions under which the G-rich strand predominantly adopts an antiparallel structure F_1) or after 8 h, when 222 is already fully folded into a parallel structure F_2 (Figure S9). The calculated rate constants k_{off} of F_1 and F_2 are 0.6510 and 0.06399 min^{-1}, respectively, indicating that the introduction of the complementary strand leads to relatively fast duplex formation and unfolding of the antiparallel intermediate structure. In contrast, duplex formation is 10-fold slower when F_2 is formed, meaning that the parallel quadruplex is more stable and less prone to unfolding than F_1.

From the perspective of activation energy, the rate constants of both forward and reverse reactions increase with the temperature. However, the reverse reaction rate constant increases faster due to the greater activation energy of the reverse reaction (Figure 3E). From a mechanistic point of view, a temperature increase is adverse to the stability of F_1, thus weakening the positive effect of the temperature on the rate constants. In other words, the decrease in stability of F_1 makes it more susceptible to conformational transitions, as shown by an increase in k_2, while k and k_1 exhibit tendencies similar to those of k_2.

In addition, the temperature effects on the folding process of 222 in Sr^{2+} (Figure S10 and Table S7) and 222T in K^+ (Figure S11 and Table S8) and Sr^{2+} (Figure S12 and Table S9) were almost the same as 222 in K^+.

Effect of Na^+ on the Antiparallel Intermediate G4 Structure. To investigate the effect of Na^+ on the antiparallel G4 structure, the folding processes of 222 under different

https://doi.org/10.1021/acs.jpcb.4c04570
J. Phys. Chem. B 2024, 128, 11077−11087

cation conditions were analyzed. As displayed in Figure 4A, 222 forms an antiparallel G4 structure in Na^+, while it converts into a parallel structure in the presence of K^+, no matter the order of Na^+ addition. The results demonstrate that K^+ can force the Na^+-form antiparallel structure to convert into a parallel topology (K^+ being also a more favorable cation for G-quadruplexes).[31] Interestingly, as observed in Figure 4B, the addition of Na^+ accelerates the folding rate of 222 to form a parallel structure. The nearly overlapped time-tracking curves of 222 in Na^+ after addition of K^+ and 222 in Na^+ and K^+ mixed solution, suggest that whether Na^+ is added earlier or not has no effect on the folding process (rate constants are shown below). These collected data indicate that Na^+ can accelerate the conformational transition process of process I, thus accelerating the whole folding process. In contrast to sequence 222, adding Na^+ did not accelerate the folding rate of d222r at room temperature (Figure 4C). In addition, the folding rate of 222 at 65 °C was independent of Na^+ (Figure 4D). These two observations here demonstrate that Na^+ has no accelerating effect on process II.

The effects of Na^+ on the folding of 222 in Sr^{2+} (Figure S13), 222T in K^+ (Figure S14), and 222T in Sr^{2+} (Figure S15) are relatively similar. All rate constants are shown in Figure 4E. Compared to Sr^{2+}, K^+ has a faster folding rate, especially in k_2 with up to a 10-fold enhancement. Among the thermodynamic constants presented in the previous section, Sr^{2+} has larger equilibrium constants and higher reaction activation energies than K^+, suggesting that the structure formed by 222/222T in Sr^{2+} is more stable.

We then followed G4 formation by 222 at different K^+ concentrations (Figure 5A). With an increase in K^+ concentration, 222 undergoes a transition from a single strand to an antiparallel structure, then to a mix, and finally to the parallel structure. Such a result indicates that when K^+ concentration is low, 222 is more likely to form an antiparallel structure that does not convert into a parallel structure, meaning that $k_2 = 0$ (since $k_1 \gg k$, so even if it can form a parallel structure through path II, its amount can be neglected).

Next, we determined the structural change of 222 in 10 μM K^+, which still forms an antiparallel topology at different temperatures (Figure 5B). As the temperature increases, the characteristic peak of the antiparallel structure at 295 nm decreases rapidly, but we do not observe the characteristic peak of the parallel structure. This result indicates that the antiparallel structure unfolds at a relatively low temperature but does not convert into a parallel structure. However, when a similar experiment is performed in 100 μM K^+, 222 forms a mixed structure at low temperatures (for instance at 5 °C in Figure 5C). Interestingly, the proportion of parallel structures increases with the temperature (Figure 5C). For example, the characteristic peak of parallel structure is present at 15, 25, and 35 °C, while single strands predominate at higher temperatures. These data suggest that, as the temperature increases, k_2 increases and the lifetime of the antiparallel structure decreases, so the proportion of parallel structures increases, which is consistent with the observations shown in Figure 3C. This phenomenon implies that the antiparallel structure can convert, but not completely, into a parallel structure. Upon further increase of the K^+ concentration to 100 mM, 222 retains a parallel structure from 5 to 75 °C (Figure 5D), meaning that k_2 is a nonzero constant.

DISCUSSION

The existing studies on G4 folding primarily focus on transient folded states and the steady-state conformation. For instance, it has been reported that cation-oligonucleotide complexes rapidly form during the folding process, followed by a gradual transition toward the final folded structure.[35] Related works also emphasize the possible contribution of G-duplexes and G-triplexes to the folding kinetics.[23] These studies predominantly center on examining various transient processes. Additionally, numerous reports have explored multiple intermediate states in the G4 folding pathway, with a particular emphasis on the initial and final conformations.[34,36,37] Herein, we investigated the effect of intermediate structures on the overall folding process. In this work, the folding processes of 222 and 222T were investigated in depth. Although 222 and 222T eventually form a stable parallel G4 structure in K^+, the first folded species to be observed is an antiparallel G4 structure, unveiled by CD. The situation is clearly different for d222r, which directly forms a parallel structure. The folding of single-stranded DNA into parallel structures may be preceded by some transient species, such as G-hairpins or G-triplexes, but these early transient species cannot be detected by stopped-flow CD due to its time limitation, as it can access only species in the millisecond time range. Our findings are consistent with the previous conclusions that K^+-driven folding is a two-step process. For instance, a work showed that G4 folding in K^+ solution by the c-*KIT* promoter sequence occurs with a short-lived antiparallel folding intermediate and a formation rate constant of 487.8 ± 20.40 min^{-1}.[38] In the present study, the rate constant of 222 in K^+ is 424.2 ± 3.016 min^{-1}, for the formation of antiparallel structures, which is very close to that observed in the c-*KIT* promoter sequences. In addition, other works also identified antiparallel intermediates, stimulating the hypothesis that antiparallel G4 structures may occur during G4 folding for most sequences (e.g., c-*KIT*,[22] Tel22 (d[AGGG-(TTAGGG)$_3$]),[38] and wt-cMYC (d-[TGGGAGGGTGGGGAGGGTGGGG]),[39] etc.), least those with a primary sequence allowing antiparallel structure formation, and a T_m of the final structure higher than the one of the antiparallel G4 structure. These studies suggest that the antiparallel structure is an intermediate in the folding process, and we probe the competing role of the antiparallel structure throughout the folding process herein.

The results collected in our study demonstrate that 222 has at least two possible routes to form a parallel G4 structure: (i) through an antiparallel G4 structure, which then slowly transforms into a parallel topology; (ii) through a direct route. In our experiments, the vast majority of single strands form antiparallel G4 structures first due to the faster formation of this antiparallel fold as compared to the parallel structure under the same conditions, suggesting that this antiparallel structure competes with the parallel form. Interestingly, our experimental results show that the rates of antiparallel G4 structure unfolding (partial or complete into a single strand) and transformation into the parallel topology are very slow. Therefore, the formation pathway via direct parallel structure folding is faster than the other indirect pathway that transits through an antiparallel structure. This indicates that the antiparallel G4 structure acts as a trap during the folding process. In other words, once an antiparallel G4 is formed, it becomes harder to form another structure. The activation energy is 68.74 KJ mol^{-1} for the unfolding of the antiparallel

https://doi.org/10.1021/acs.jpcb.4c04570
J. Phys. Chem. B 2024, 128, 11077−11087

structure and 117.1 KJ mol^{-1} for the folding of the antiparallel structure into the parallel structure (Figure 6). The activation

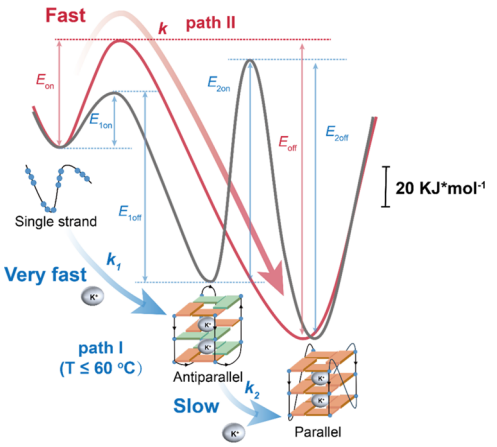

Figure 6. Energy landscape of 222 folding in 100 mm K$^+$ at 25 °C. The formation of a parallel G-quadruplex from a single strand via two paths: one forms an antiparallel G-quadruplex first and then transforms into parallel topology (path I); the other forms a parallel structure directly in path II. The activation energy of path I is 68.74 KJ mol^{-1} for the unfolding of the antiparallel structure and 117.1 KJ mol^{-1} for the folding of the antiparallel structure into the parallel structure, whereas that of path II is 53.71 KJ mol^{-1}.

energy of folding directly into the parallel structure from single-strand folding is 53.71 KJ mol^{-1}, which is much lower than the two activation energies listed above (Figure 6). These results reveal that once the antiparallel structure is formed, it is difficult to unfold on the one hand, and to form a parallel structure on the other hand; thus, the appearance of the antiparallel G4 structure greatly slows down the folding rate. So, the antiparallel structure acts as a trap during folding (Figure 6). However, it should be noted that antiparallel G4 structures do not always prevent the folding,[26,39] as it depends on the sequence and environmental factors. Interestingly, k_2 (the conversion rate of antiparallel to parallel G4 structures in path II) increases with temperature faster than k (the rate at which single strands fold into parallel structures in path I). This result implies that a temperature may exist, for which k_2 is greater than k, that is, folding through path I becomes faster than folding through path II. It is worth noting that a probability that the antiparallel G4 structure cannot exist because of its low T_m value. For instance, k_2 is almost the same as k at 60 °C, indicating that the rates of folding through both pathways are similar, so the antiparallel G4 structure no longer acts as a folding trap during G4 formation. However, at temperatures lower than the T_m of the antiparallel structure, the two formation pathways are still in competition due to the extremely fast formation rate of the antiparallel G4 structure.

G4s are very sensitive to cations, and we also demonstrated that the introduction of Na$^+$ accelerates the conformational transition of antiparallel to parallel G4 (Figure 4B). This observation is consistent with previous findings on human telomeric repeats, where a faster folding rate in Na$^+$ is observed. It was proposed that the accessibility of the cation to the interior of the partially folded intermediate has an important influence on the rate of folding.[35] Herein, we propose that the acceleration induced by Na$^+$ may result from specific binding of Na$^+$ to the antiparallel G4 structure, which facilitates the conformational transition process, thus accelerating the entire folding process from a single strand to parallel G4. In addition, the comparison of folding processes of 222 and 222T in K$^+$ and Sr^{2+} demonstrates that k_1 is not necessarily related to the species of metal ions.

Finally, we followed the G4 formation at different K$^+$ concentrations. With increasing potassium concentrations, we observed that 222 underwent a transition from a single-strand to an antiparallel structure, then to a mix, and finally to the parallel structure. We suspect that there is a minimum K$^+$ concentration below which 222 cannot form parallel structures ($k_2 = 0$), and a maximum K$^+$ concentration above which 222 can form parallel structures only ($k_2 \neq 0$). However, when the concentration of K$^+$ is between these two critical concentrations, there is a balance between the parallel and antiparallel structures, and the proportion of the two will also change with temperature. These analyses reveal that the antiparallel structure is not a necessary intermediate structure for folding to form a parallel structure but rather a folding trap. For instance, it will never form a parallel structure at a low concentration of K$^+$.

CONCLUSIONS

We report here the folding process of 222 and 222T and find two formation pathways for both sequences, with parallel G4s as the end conformation. One pathway consists of a direct parallel G4 structure formation, while the other proceeds through an antiparallel G4 intermediate. A detailed analysis reveals that the presence of an antiparallel structure exerts a significant competitive effect during the folding process, effectively hindering the formation of parallel G4 structures. As such, the antiparallel structure functions more as a dead end rather than a transitional intermediate. Exploring the characteristics of folding intermediate structures broadens our understanding of the factors influencing G4 folding processes.

ASSOCIATED CONTENT

Supporting Information

The Supporting Information is available free of charge at https://pubs.acs.org/doi/10.1021/acs.jpcb.4c04570.

Additional experimental data; kinetic curve fitting and corresponding residual plot of 10 μM 222 in the presence of 100 mM K$^+$, ellipticity is recorded at 264 nm, from left to right: 5 s, 2, and 30 min; melting and annealing curves of 5 mM 222 in 100 μM K$^+$ at 295 nm, the experiment was performed in 10 mM Tris-HCl buffer (pH 7); dynamic folding process models, and folding rate constant and number of stages of 10 μM 222 in 100 mM Sr^{2+} at different temperatures (PDF)

AUTHOR INFORMATION

Corresponding Author

Jun Zhou − *State Key Laboratory of Analytical Chemistry for Life Science, School of Chemistry & Chemical Engineering, Nanjing University, Nanjing 210023, China;* orcid.org/0000-0002-6793-3169; Email: jun.zhou@nju.edu.cn

Authors

Jianjun Xia − *State Key Laboratory of Analytical Chemistry for Life Science, School of Chemistry & Chemical Engineering, Nanjing University, Nanjing 210023, China*

Jielin Chen − *State Key Laboratory of Analytical Chemistry for Life Science, School of Chemistry & Chemical*

https://doi.org/10.1021/acs.jpcb.4c04570
J. Phys. Chem. B 2024, 128, 11077−11087

Engineering, Nanjing University, Nanjing 210023, China; orcid.org/0000-0003-4930-2870

Jiahang Zhou − *State Key Laboratory of Analytical Chemistry for Life Science, School of Chemistry & Chemical Engineering, Nanjing University, Nanjing 210023, China*

Mingpan Cheng − *School of Engineering, China Pharmaceutical University, Nanjing 211198, China;* orcid.org/0000-0003-1282-0076

Xinzhe Zhuang − *State Key Laboratory of Analytical Chemistry for Life Science, School of Chemistry & Chemical Engineering, Nanjing University, Nanjing 210023, China*

Chengfeng Cai − *State Key Laboratory of Analytical Chemistry for Life Science, School of Chemistry & Chemical Engineering, Nanjing University, Nanjing 210023, China*

Huangxian Ju − *State Key Laboratory of Analytical Chemistry for Life Science, School of Chemistry & Chemical Engineering, Nanjing University, Nanjing 210023, China;* orcid.org/0000-0002-6741-5302

Jean-Louis Mergny − *State Key Laboratory of Analytical Chemistry for Life Science, School of Chemistry & Chemical Engineering, Nanjing University, Nanjing 210023, China; Laboratoire d'Optique et Biosciences, Ecole Polytechnique, CNRS, INSERM, Institut Polytechnique de Paris, 91120 Palaiseau, France;* orcid.org/0000-0003-3043-8401

Complete contact information is available at: https://pubs.acs.org/10.1021/acs.jpcb.4c04570

Author Contributions

[‖]J.X. and J.C. contributed equally to this work.

Notes

The authors declare no competing financial interest.

■ ACKNOWLEDGMENTS

This work was supported by the National Natural Science Foundation of China (22177047, 22307143, and 22374070), the State Key Laboratory of Analytical Chemistry for Life Science (5431ZZXM2406), and the Fundamental Research Funds for the Central Universities (020514380299).

■ REFERENCES

(1) Mendoza, O.; Bourdoncle, A.; Boulé, J.-B.; Brosh, R. M.; Mergny, J.-L. G-quadruplexes and helicases. *Nucleic Acids Res.* **2016**, *44* (5), 1989−2006.

(2) Mergny, J.-L.; Sen, D. DNA quadruple helices in nanotechnology. *Chem. Rev.* **2019**, *119* (10), 6290−6325.

(3) Nakano, S.-i.; Miyoshi, D.; Sugimoto, N. Effects of molecular crowding on the structures, interactions, and functions of nucleic acids. *Chem. Rev.* **2014**, *114* (5), 2733−2758.

(4) Robinson, J.; Raguseo, F.; Nuccio, S. P.; Liano, D.; Di Antonio, M. DNA G-quadruplex structures: more than simple roadblocks to transcription? *Nucleic Acids Res.* **2021**, *49* (15), 8419−8431.

(5) Lam, E. Y. N.; Beraldi, D.; Tannahill, D.; Balasubramanian, S. G-quadruplex structures are stable and detectable in human genomic DNA. *Nat. Commun.* **2013**, *4*, No. 1796.

(6) Cadoni, E.; De Paepe, L.; Manicardi, A.; Madder, A. Beyond small molecules: targeting G-quadruplex structures with oligonucleotides and their analogues. *Nucleic Acids Res.* **2021**, *49* (12), 6638−6659.

(7) Platella, C.; Riccardi, C.; Montesarchio, D.; Roviello, G. N.; Musumeci, D. G-quadruplex-based aptamers against protein targets in therapy and diagnostics. *Biochim. Biophys. Acta, Gen. Subj.* **2017**, *1861* (5), 1429−1447.

(8) Zhang, Y.; Cheng, Y.; Luo, Q.; Wu, T.; Huo, J.; Yin, M.; Peng, H.; Xiao, Y.; Tong, Q.; You, H. Distinguishing G-quadruplexes stabilizer and chaperone for c-MYC promoter G-quadruplexes through single-molecule manipulation. *J. Am. Chem. Soc.* **2024**, *146* (6), 3689−3699.

(9) Ren, L.; Zhang, A.; Huang, J.; Wang, P.; Weng, X.; Zhang, L.; Liang, F.; Tan, Z.; Zhou, X. Quaternary ammonium zinc phthalocyanine: inhibiting telomerase by stabilizing G quadruplexes and inducing G-quadruplex structure transition and formation. *ChemBioChem* **2007**, *8* (7), 775−780.

(10) Petraccone, L.; Spink, C.; Trent, J. O.; Garbett, N. C.; Mekmaysy, C. S.; Giancola, C.; Chaires, J. B. Structure and stability of higher-order human telomeric quadruplexes. *J. Am. Chem. Soc.* **2011**, *133* (51), 20951−20961.

(11) Nguyen, T. Q. N.; Lim, K. W.; Phan, A. T. Folding kinetics of G-quadruplexes: Duplex stem loops drive and accelerate G-quadruplex folding. *J. Phys. Chem. B* **2020**, *124* (25), 5122−5130.

(12) Bhattacharyya, D.; Arachchilage, G. M.; Basu, S. Metal cations in G-quadruplex folding and stability. *Front. Chem.* **2016**, *4*, No. 38.

(13) Cragnolini, T.; Chakraborty, D.; Šponer, J.; Derreumaux, P.; Pasquali, S.; Wales, D. J. Multifunctional energy landscape for a DNA G-quadruplex: An evolved molecular switch. *J. Chem. Phys.* **2017**, *147*, No. 152715.

(14) McCarte, B.; Yeung, O. T.; Speakman, A. J.; Elfick, A.; Dunn, K. E. Using ultraviolet absorption spectroscopy to study nanoswitches based on non-canonical DNA structures. *Biochem. Biophys. Rep.* **2022**, *31*, No. 101293.

(15) Cheng, M.; Cheng, Y.; Hao, J.; Jia, G.; Zhou, J.; Mergny, J.-L.; Li, C. Loop permutation affects the topology and stability of G-quadruplexes. *Nucleic Acids Res.* **2018**, *46* (18), 9264−9275.

(16) Klejevskaja, B.; Pyne, A. L. B.; Reynolds, M.; Shivalingam, A.; Thorogate, R.; Hoogenboom, B. W.; Ying, L.; Vilar, R. Studies of G-quadruplexes formed within self-assembled DNA mini-circles. *Chem. Commun.* **2016**, *52* (84), 12454−12457.

(17) Aznauryan, M.; Søndergaard, S.; Noer, S. L.; Schiøtt, B.; Birkedal, V. A direct view of the complex multi-pathway folding of telomeric G-quadruplexes. *Nucleic Acids Res.* **2016**, *44* (22), 11024−11032.

(18) Soenarjo, A. L.; Lan, Z.; Sazanovich, I. V.; Chan, Y. S.; Ringholm, M.; Jha, A.; Klug, D. R. The transition from unfolded to folded G-quadruplex DNA analyzed and interpreted by two-dimensional infrared spectroscopy. *J. Am. Chem. Soc.* **2023**, *145* (36), 19622−19632.

(19) You, H.; Wu, J.; Shao, F.; Yan, J. Stability and kinetics of c-MYC promoter G-quadruplexes studied by single-molecule manipulation. *J. Am. Chem. Soc.* **2015**, *137* (7), 2424−2427.

(20) Liu, W.; Fu, Y.; Zheng, B.; Cheng, S.; Li, W.; Lau, T.-C.; Liang, H. Kinetics and mechanism of conformational changes in a G-quadruplex of thrombin-binding aptamer induced by Pb^{2+}. *J. Phys. Chem. B* **2011**, *115* (44), 13051−13056.

(21) Laouer, K.; Schmid, M.; Wien, F.; Changenet, P.; Hache, F. Folding dynamics of DNA G-quadruplexes probed by millisecond temperature jump circular dichroism. *J. Phys. Chem. B* **2021**, *125* (29), 8088−8098.

(22) Gray, R. D.; Trent, J. O.; Chaires, J. B. Folding and unfolding pathways of the human telomeric G-quadruplex. *J. Mol. Biol.* **2014**, *426* (8), 1629−1650.

(23) Zhang, M.-L.; Xu, Y.-P.; Kumar, A.; Zhang, Y.; Wu, W.-Q. Studying the potassium-induced G-quadruplex DNA folding process using microscale thermophoresis. *Biochemistry* **2019**, *58* (38), 3955−3959.

(24) Stadlbauer, P.; Kührová, P.; Vicherek, L.; Banáš, P.; Otyepka, M.; Trantírek, L.; Šponer, J. Parallel G-triplexes and G-hairpins as potential transitory ensembles in the folding of parallel-stranded DNA G-quadruplexes. *Nucleic Acids Res.* **2019**, *47* (14), 7276−7293.

(25) Carrino, S.; Hennecker, C. D.; Murrieta, A. C.; Mittermaier, A. Frustrated folding of guanine quadruplexes in telomeric DNA. *Nucleic Acids Res.* **2021**, *49* (6), 3063−3076.

(26) Harkness, R. W.; Hennecker, C.; Grün, J. T.; Blümler, A.; Heckel, A.; Schwalbe, H.; Mittermaier, A. K. Parallel reaction

pathways accelerate folding of a guanine quadruplex. *Nucleic Acids Res.* **2021**, *49* (3), 1247−1262.
(27) Bončina, M.; Vesnaver, G.; Chaires, J. B.; Lah, J. Unraveling the thermodynamics of the folding and interconversion of human telomere G-quadruplexes. *Angew. Chem., Int. Ed.* **2016**, *55* (35), 10340−10344.
(28) Gray, R. D.; Chaires, J. B. Kinetics and mechanism of K^+- and Na^+-induced folding of models of human telomeric DNA into G-quadruplex structures. *Nucleic Acids Res.* **2008**, *36* (12), 4191−4203.
(29) Marchand, A.; Gabelica, V. Folding and misfolding pathways of G-quadruplex DNA. *Nucleic Acids Res.* **2016**, *44* (22), 10999−11012.
(30) Chen, J.; Cheng, M.; Stadlbauer, P.; Šponer, J.; Mergny, J.-L.; Ju, H.; Zhou, J. Exploring sequence space to design controllable G-quadruplex topology switches. *CCS Chem.* **2022**, *4* (9), 3036−3050.
(31) Largy, E.; Marchand, A.; Amrane, S.; Gabelica, V.; Mergny, J.-L. Quadruplex turncoats: Cation-dependent folding and stability of quadruplex-DNA double switches. *J. Am. Chem. Soc.* **2016**, *138* (8), 2780−2792.
(32) Tang, C.-F.; Shafer, R. H. Engineering the Quadruplex Fold: Nucleoside Conformation Determines Both Folding Topology and Molecularity in Guanine Quadruplexes. *J. Am. Chem. Soc.* **2006**, *128* (17), 5966−5973.
(33) Liu, W.; Zhu, H.; Zheng, B.; Cheng, S.; Fu, Y.; Li, W.; Lau, T. C.; Liang, H. Kinetics and mechanism of G-quadruplex formation and conformational switch in a G-quadruplex of PS2.M induced by Pb^{2+}. *Nucleic Acids Res.* **2012**, *40* (9), 4229−4236.
(34) Chaires, J. B. Human telomeric G-quadruplex: thermodynamic and kinetic studies of telomeric quadruplex stability. *FEBS J.* **2010**, *277* (5), 1098−1106.
(35) Lane, A. N.; Chaires, J. B.; Gray, R. D.; Trent, J. O. Stability and kinetics of G-quadruplex structures. *Nucleic Acids Res.* **2008**, *36* (17), 5482−5515.
(36) Gray, R. D.; Li, J.; Chaires, J. B. Energetics and kinetics of a conformational switch in G-quadruplex DNA. *J. Phys. Chem. B* **2009**, *113*, 2676−2683.
(37) Gray, R. D.; Buscaglia, R.; Chaires, J. B. Populated intermediates in the thermal unfolding of the human telomeric quadruplex. *J. Am. Chem. Soc.* **2012**, *134* (40), 16834−16844.
(38) Rigo, R.; Dean, W. L.; Gray, R. D.; Chaires, J. B.; Sissi, C. Conformational profiling of a G-rich sequence within the c-KIT promoter. *Nucleic Acids Res.* **2017**, *45* (22), 13056−13067.
(39) Grün, J. T.; Blümler, A.; Burkhart, I.; Wirmer-Bartoschek, J.; Heckel, A.; Schwalbe, H. Unraveling the kinetics of spare-tire DNA G-quadruplex folding. *J. Am. Chem. Soc.* **2021**, *143* (16), 6185−6193.

https://doi.org/10.1021/acs.jpcb.4c04570
J. Phys. Chem. B 2024, 128, 11077−11087